Available online at www.sciencedirect.com
SCIENCE DIRECT®
Journal of volcanology and geothermal research
ELSEVIER
Journal of Volcanology and Geothermal Research 121 (2003) 247–269
www.elsevier.com/locate/jvolgeores

Petrographic features of a high-temperature granite just newly solidified magma at the Kakkonda geothermal field, Japan

Munetake Sasaki [a,*], Koichiro Fujimoto [a], Takayuki Sawaki [a], Hitoshi Tsukamoto [a], Osamu Kato [b], Ryo Komatsu [b], Nobuo Doi [b], Masakatsu Sasada [a]

[a] *Geological Survey of Japan, AIST, Higashi 1-1-1, Tsukuba, Ibaraki 305-8567, Japan*
[b] *Japan Metals and Chemicals Co. Ltd., Sasamori 72, Ukai, Takizawa, Iwate 020-0172, Japan*

Received 25 June 2001; received in revised form 7 August 2002; accepted 7 August 2002

Abstract

A 3729-m-deep geothermal research well, WD-1a, provides us with a unique opportunity to study initial petrographic features of a high-temperature granite just after solidification of magma. The well succeeded in collecting three spot-cores of the Kakkonda Granite that is a pluton emplaced at a shallow depth and regarded as a heat source of the active Kakkonda geothermal system. The core samples were collected at the present formation temperatures of 370, 410 and over 500°C. These samples are granodiorite to tonalite consisting mainly of plagioclase, quartz, hornblende, biotite and K-feldspar. A sample collected at a formation temperature of over 500°C possesses the following remarkable petrographic features compared to the other two samples. Interstitial spaces are not completely sealed. K-feldspar exhibits no perthite by the exsolution of albite lamella. Quartz includes glassy melt inclusions without devitrification. Hornblende is less intensively altered to actinolite, and biotite is not altered. This study directly confirmed that perthite in K-feldspar is a recrystallization texture formed at 410–500°C based on a comparison of the in situ temperatures of the samples. Chemical compositions of minerals were analyzed to compare temperatures determined from geothermometers in several publications to the in situ temperatures of the samples.

Keywords: grain boundary; perthite; glass inclusion; geologic thermometer; granite; geothermal field; Kakkonda; Japan

1. Introduction

Granites have undergone various geological events in their long cooling histories before exposure to the surface. Geological processes such as recrystallization, alteration and deformation could change the primary texture and mineral chemistry of granites formed just after the solidification of magma (e.g. Tuttle and Bowen, 1958). At the Kakkonda geothermal field in northeast Japan, the New Energy and Industrial Technology Development Organization (NEDO) drilled a deep geothermal research well, WD-1a (total depth: 3729 m), to investigate potential deep geothermal resources (Sasada et al., 1993; Muraoka

* Corresponding author. Tel.: +81-298-61-3899; Fax: +81-298-61-3717.
E-mail address: sasaki-munetake@aist.go.jp (M. Sasaki).

0377-0273/02/$ – see front matter
PII: S0377-0273(02)00428-6

et al., 1998). The well penetrated into the Kakkonda Granite, regarded as the heat source of the geothermal system (Doi et al., 1998), and collected three spot-cores at depths with temperatures of 370, 410 and over 500°C (Nos. 11, 12 and 13 cores, respectively, of Uchida et al., 1996). Thus, the samples provided us with a unique opportunity to study initial petrographic features of granite formed just after the solidification of magma. This study describes the petrography and mineral chemistry of the samples, and compares temperatures determined from geothermometers in several publications to the in situ temperatures of the samples.

2. Geology of the Kakkonda geothermal field

At the Kakkonda geothermal field, two geothermal power plants with a total capacity of 80 MW_e are in operation (Fig. 1). The surface and subsurface geology of the field has been studied by Kato and Doi (1993), Kato and Sato (1995), Uchida et al. (1996) and Doi et al. (1998), as shown in Figs. 1 and 2. Pre-Tertiary formations are composed of slate, sandstone and andesitic tuff (Fig. 2). Tertiary formations are mainly of andesitic to dacitic tuff, tuffaceous sandstone and black shale. Rhyolitic to dacitic welded tuffs of Pleistocene age unconformably overlie the Ter-

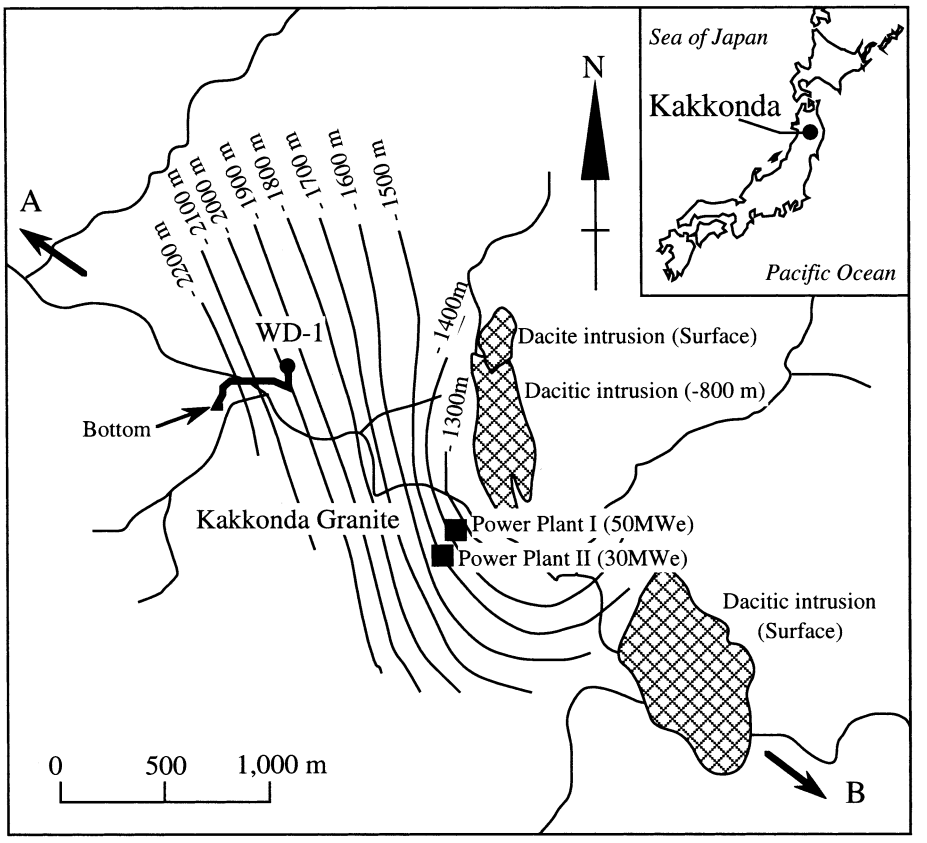

Fig. 1. Locality of the Kakkonda geothermal field with distribution of intrusions and trajectory of a deep geothermal research well, WD-1a, modified after Uchida et al. (1996). The contours indicate the top of the Kakkonda granitic body (in relation to sea level). Arrows with 'A' and 'B' correspond to the cross section in Fig. 2.

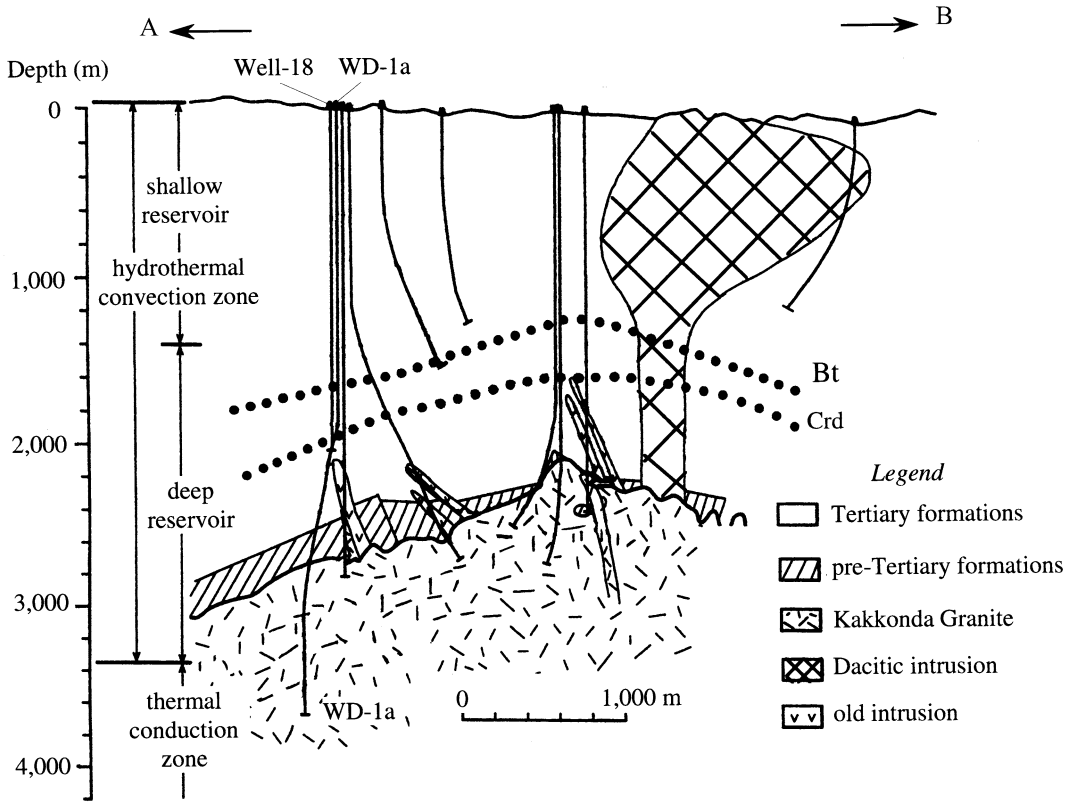

Fig. 2. A schematic cross section of the Kakkonda geothermal system, simplified after Doi et al. (1998). The cross section corresponds to the line A–B in Fig. 1. Well WD-1a penetrated 870 m into the granitic body, while several deep wells have encountered the top of the body. Abbreviations Bt and Crd indicate the shallowest depths at which metamorphic biotite and cordierite appear, respectively.

tiary formations. Andesitic volcanic rocks of Pleistocene–Holocene age cover the northeastern and southwestern parts of the field. Several dacitic intrusions are found in the Tertiary rocks. The Quaternary Kakkonda Granite has intruded in the pre-Tertiary and Tertiary rocks.

2.1. Kakkonda Granite

The Kakkonda Granite has been discovered below 2100 m depth in an area of 1.5×1.3 km with elongation in the N10–20°W direction (Uchida et al., 1996; Doi et al., 1998; Figs. 1 and 2). Well WD-1a and several other deep wells have encountered the top of the granitic body, and well WD-1a drilled 870 m into the body (Fig. 2). The granitic rocks from other deep wells were petrologically and mineralogically investigated by Kanisawa et al. (1994) and Doi et al. (1998). The Kakkonda Granite is made up of granite to quartz diorite and belongs to I-type and magnetite-series granitoid based on classifications of Chappell and White (1974) and Ishihara (1977), respectively. The K–Ar ages of the granitic rocks are from 0.24 to 0.11 Ma within an analysis error of ± 0.26 Ma for hornblende, from 0.21 to 0.02 Ma within ± 0.06 Ma for biotite and from 0.14 to 0.01 Ma within ± 0.07 Ma for K-feldspar (Doi et al., 1998). The SiO_2 contents of the granitic rocks are from 65 to 75% (Doi et al., 1998). Kanisawa et al. (1994) suggested a genetic relationship between the Kakkonda Granite and the Pleistocene

welded tuffs or Pleistocene–Holocene volcanic rocks based on the similarity in the minor element geochemistry of the rocks.

2.2. Contact metamorphism

A contact metamorphic aureole with a 1-km width is found above the Kakkonda Granite (Fig. 2). Major metamorphic minerals identified in the contact aureole are biotite, cordierite, anthophyllite, orthopyroxene, andalusite and K-feldspar (Kato and Sato, 1995). Minor amounts of corundum and spinel are also found at the immediate contact (Sawaki et al., 2001). Isograds of biotite and cordierite are almost parallel to the shape of the top of the granitic body (Fig. 2). Metamorphic temperatures at the isograds are estimated to be 397°C for biotite, 493°C for cordier-

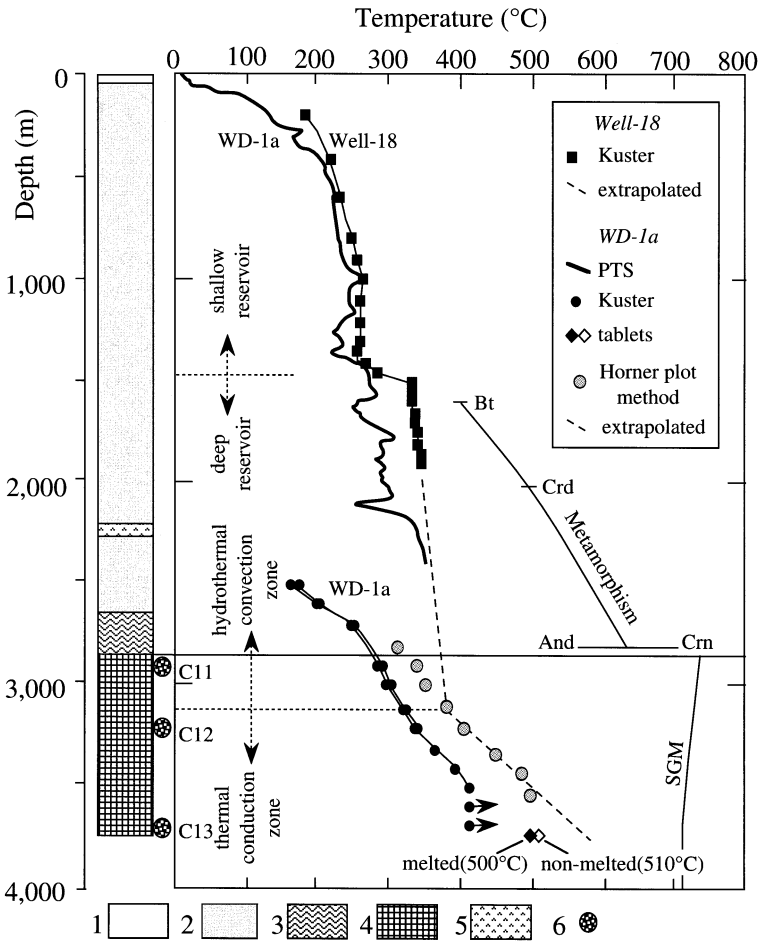

Fig. 3. Temperature profiles of well WD-1a and well-18 with a simplified geological column of well WD-1a, modified after Uchida et al. (1996) and Ikeuchi et al. (1998). 'Metamorphism' indicates a possible metamorphic temperature at the peak metamorphism with the shallowest levels at which biotite (Bt), cordierite (Crd), andalusite (And) and corundum (Crn) appear (Uchida et al., 1996; Sawaki et al., 2001; Takeno et al., 2001). A solidus of a hydrous granitic melt (SGM) is calculated using a rock density of 2.5 g/cm^3, after Tuttle and Bowen (1958). PTS: a logging tool for pressure, temperature and spinner worked below 310°C; Kuster: a temperature-logging tool with mechanical recorder and clock timer worked below 414°C; Horner plot method: a method to calculate a final static formation temperature based on increased rates of the logged temperatures with time. Legend: 1, Detritus; 2, Tertiary formations; 3, pre-Tertiary formations; 4, Kakkonda Granite; 5, old intrusions; 6, sampling point.

ite and 566°C for andalusite through a thermodynamic calculation of the metamorphic mineral assemblages (Takeno et al., 2001; Fig. 3). Mineral assemblages of corundum and K-feldspar indicate a temperature of 600–700°C at the highest grade (Sawaki et al., 2001; Fig. 3).

2.3. Present thermal structure

Geothermal-fluid productive zones in the Kakkonda field are classified into two reservoirs (the shallow and deep reservoirs; Fig. 2) based on a temperature inflection at about 1500 m depth, which is typically shown in a temperature profile of well-18 (Ikeuchi et al., 1998; Fig. 3). The reservoir temperatures are 230–260°C in the shallow reservoir and 300–350°C in the deep reservoir (Kato and Doi, 1993). The two reservoirs are hydrologically connected (Hanano, 1998). The thermal inflection at about 1500 m depth is considered to be formed by the difference in permeability of the reservoir rocks: easily permeable altered rocks in the shallow reservoir and hardly impermeable metamorphosed rocks in the deep reservoir (Hanano, 1998). The thermal structure inside the granitic body has not been fully investigated during the drilling operation of well WD-1a. The temperatures logged by the Kuster tools were at the temperature recovery stages (Fig. 3). The highest measured temperature, which was by metallic tablets, was 500°C at the bottom level (Fig. 3). Ikeuchi et al. (1998) calculated final static formation temperatures based on the increased rates of the logged temperatures with time (Horner plot method; Fig. 3). They compared the calculated temperatures to extrapolated temperatures from the deep reservoir downward and concluded that the hydrothermal convection zone ceases at 3100 m depth and the thermal conduction zone prevails underneath the hydrothermal convection zone (Fig. 3). The thermal conduction zone is calculated to have a steep temperature gradient of 32°C/100 m from 380°C at 3100 m depth to 500°C at 3500 m depth (Ikeuchi et al., 1998; Fig. 3).

Geothermal fluids produced from shallow and deep reservoirs are meteoric in origin (Yanagiya et al., 1996) and circulate under a condition close to the boiling point with a depth curve of water. A minor amount of meteoric water has already infiltrated down to a 3250 m depth in the granitic body through narrow fractures based on studies of fluid inclusions and stable isotopes (Ikeuchi et al., 1998; Komatsu et al., 1998; Kasai et al., 2000; Kato et al., 2000). However, the narrow fractures seem to lack the amount and connectivity needed to cause effective hydrothermal convection below 3100 m depth. Below a depth of 3350 m, fluids trapped in the granitic body are rich in CO_2 and H_2S gases (Ikeuchi et al., 1998; Kasai et al., 1998). At the bottom level of well WD-1a, fluids trapped in the granitic body are hypersaline, as sampled by the fluid circulation test at well WD-1a (Kasai et al., 1998).

3. Petrography of the samples

3.1. Description of granitic rocks

The petrography of the three core samples from well WD-1a (Nos. 11, 12 and 13 cores; Uchida et al., 1996) is summarized in Table 1.

The No. 11 core sample (C11) was collected at 2936–2939 m depth. The present formation temperature at this depth is determined to be 370°C through the extrapolation of deep reservoir temperatures to this depth (Fig. 3). The C11 is granodiorite with a weak porphyritic texture and composed mainly of plagioclase, quartz, hornblende and biotite (Table 1). Small amounts of K-feldspar, quartz, albite and biotite are found as interstitial minerals, and magnetite, apatite, titanite and zircon are accessory minerals. Miarolitic cavities of about 5 mm in diameter are sporadically distributed in the rock, and quartz, K-feldspar and hornblende are found in the cavities.

The No. 12 core sample (C12) was collected at 3228–3231 m depth (Table 1). The present formation temperature at this depth was calculated to be 410°C through the Horner plot method (Fig. 3). A minor amount of meteoric water has already infiltrated to this depth based on fluid inclusion and stable isotope studies (Ikeuchi et al., 1998; Komatsu et al., 1998; Kasai et al., 2000; Kato et al., 2000). The C12 is tonalite with a granophy-

Table 1
A summary of petrographic features of the Kakkonda Granite

Core name:	C11	C12	C13
	Granodiorite	Tonalite	Tonalite
Sampling depth:	2936–2939 m	3228–3231 m	3726–3729 m
	370°C	410°C	over 500°C
Petrography			
Texture	weak porphyritic texture miarolitic cavity	granophyric texture	equigranular
Minerals	major: Pl, Qtz, Hbl, Bt interstitial: Kfs, Qtz, Bt, Ab accessory: Mag, Ap, Ttn, Zrn	major: Pl, Qtz, Hbl, Bt interstitial: Kfs, Qtz, Bt accessory: Mag, Py, Ap, Zrn	major: Pl, Qtz, Hbl, Bt minor: Kfs accessory: Mag, Py, Ap, Zrn
Mineralogy			
Pl	core–mantle–rim inclusions core: Cpx, Opx, Mag, Ap mantle: dev.MI rim: fluid inclusions (many) sealed microfractures	core–mantle–rim inclusions core: Cpx, Mag, Ap mantle: dev.MI sealed microfractures	core–mantle, no rim inclusions core: Opx, Cpx, Mag, Ap mantle: Kfs, unidentified minerals
Kfs	perthite (commonly found) fluid inclusion (many)	perthite (sparcely found) fluid inclusion (many)	no perthite fluid inclusion (a few)
Qtz	inclusions Fe–Ti oxides, Ap FI (many), Types: L, V, P FI healed plane: frequently identified wavy extinction	inclusions Fe–Ti oxides, Ap FI (many), Types: L, V, P FI healed plane: rarely identified wavy extinction, subgrain boundary	inclusions Core: Fe–Ti oxides, MI (many) Periphery: MI FI (many), Types: V, P FI healed plane: seldom identified wavy extinction, subgrain boundary
Hbl	coarse grains: Mg-Hbl, Act (partly) inclusion: Cpx fibrous grains: Act	coarse grains: Mg-Hbl, Act (partly) inclusion: Cpx	coarse grains: Mg-Hbl, Act (partly) inclusion: Opx, Cpx (, Cum)
Bt	platy, flaky	platy, flaky	platy
Mag			ilmenite lamella
Other			free interstitial spaces

Abbreviations: Ab, albite; Act, actinolite; Ap, apatite; Bt, biotite; Cpx, clinopyroxene; Cum, cummingtonite; Hbl, hornblende; Kfs, K-feldspar; Mag, magnetite; Opx, orthopyroxene; Pl, plagioclase; Py, pyrite; Qtz, quartz; Ttn, titanite; Zrn, zircon; dev., devitrified; MI, melt inclusion; Mg, magnesio; FI, fluid inclusion, which is classified into the three types of liquid-rich two-phase (L), vapor-rich two-phase (V) and polyphase (P).

ric texture and composed mainly of plagioclase, quartz, hornblende and biotite (Table 1). Small amounts of K-feldspar, quartz and biotite are found as interstitial minerals, and magnetite, pyrite, apatite and zircon are accessory minerals. A quartz vein of 1 cm in width is observed in the sample.

The No. 13 core sample (C13) was collected at 3726–3729 m depth (Table 1). The formation temperature at this depth was measured to be 500°C by the metallic tablets (Fig. 3). The C13 is equigranular tonalite composed mainly of plagioclase, quartz, hornblende and biotite (Table 1). A small amount of K-feldspar is found as an interstitial mineral, and magnetite, pyrite, apatite and zircon are accessory minerals. A quartz vein less than 2 cm in width is found in the sample. The surface of C13 is rough, in contrast to C11 and C12, due to the presence of free interstitial spaces, as described below, and artificial generation of horizontal microcracks with vertical intervals of 2 mm to 2 cm during retrieval of the core.

Dioritic enclaves ranging from 0.5 to 10 cm in diameter sporadically occur in the three samples. The enclaves are composed mainly of plagioclase, hornblende and magnetite in C11, orthopyroxene, plagioclase, hornblende and magnetite with small amounts of biotite and quartz in C12 and plagioclase, hornblende, biotite and K-feldspar in C13.

3.2. Description of minerals and free interstitial spaces

The mineralogy of the samples is summarized in Table 1.

Plagioclase in the samples occurs as euhedral to subhedral grains and consists of an irregularly shaped core with patchy zoning in the mantle with oscillatory zoning (Fig. 4a,b). The mantles are surrounded or partly replaced by albite-rich rims in C11 and C12 (Fig. 4a), but not in C13 (Fig. 4b). The rims of plagioclase fade into zones of albite lamellae in interstitial K-feldspar in C11 and C12 (Fig. 4c), while plagioclase contacts with interstitial K-feldspar at sharp surfaces in C13 (Fig. 4d). Plagioclase includes fine grains of pyroxene, magnetite and apatite at its core. Pairs of orthopyroxene and clinopyroxene are found at the cores of plagioclase in C11 and C13, but only clinopyroxene in C12. Mantles of plagioclase include devitrified melt inclusions, K-feldspar and fine unidentified minerals along crystal growth planes. A set of devitrified melt inclusions exhibits variable volume ratios of bubbles to crystals. Rims of plagioclase include many fluid inclusions in C11. Sealed microfractures are rarely observed in plagioclase of C11 and C12 (Fig. 4e), and are not present in C13.

Interstitial K-feldspar in only C11 and C12 exhibits perthite by exsolution of albite lamella (Fig. 4c), but no perthite in C13 (Fig. 4d). Interstitial K-feldspar rarely exhibits granophyric textures with quartz in C12. Fluid inclusions are frequently found in K-feldspar of C11 and C12, but seldom in C13.

Quartz in C11 and C12 rarely includes fine needle-like grains of apatite and Fe–Ti oxide grains less than 50 μm in length. Quartz in C13 includes many Fe–Ti oxide grains and melt inclusions at its core and a few melt inclusions at its periphery. The melt inclusions have spherical shapes or negative crystal shapes of β-quartz (Fig. 4i), and occur randomly or form clusters in quartz. The sizes of the melt inclusions are less than 1 μm at the core and less than 50 μm at the periphery. Melt inclusions commonly consist of a glass phase with or without a bubble and rarely include a few tiny unidentified crystals. All quartz in the samples includes many fluid inclusions less than 60 μm. The shapes of the fluid inclusions are almost spherical, ellipsoidal, or are negative crystal shapes of α-quartz or α-quartz close to β-quartz. The fluid inclusions are classified into three types (Fig. 4j): liquid-rich two-phase, vapor-rich two-phase and polyphase inclusions. The polyphase inclusion contains halite as a major daughter mineral and iron-bearing chloride. The liquid-rich inclusions are found in C11 and C12, and vapor-rich and polyphase inclusions are found in all three samples. Fluid inclusion healed planes are frequently identified in C11, rarely in C12 and seldom in C13. Quartz in the samples rarely exhibits weak wavy extinction and subgrain boundaries. The subgrain boundaries typically occur normal to the *c*-axes of quartz in C12 and C13.

Orthopyroxene in coarse hornblende is sur-

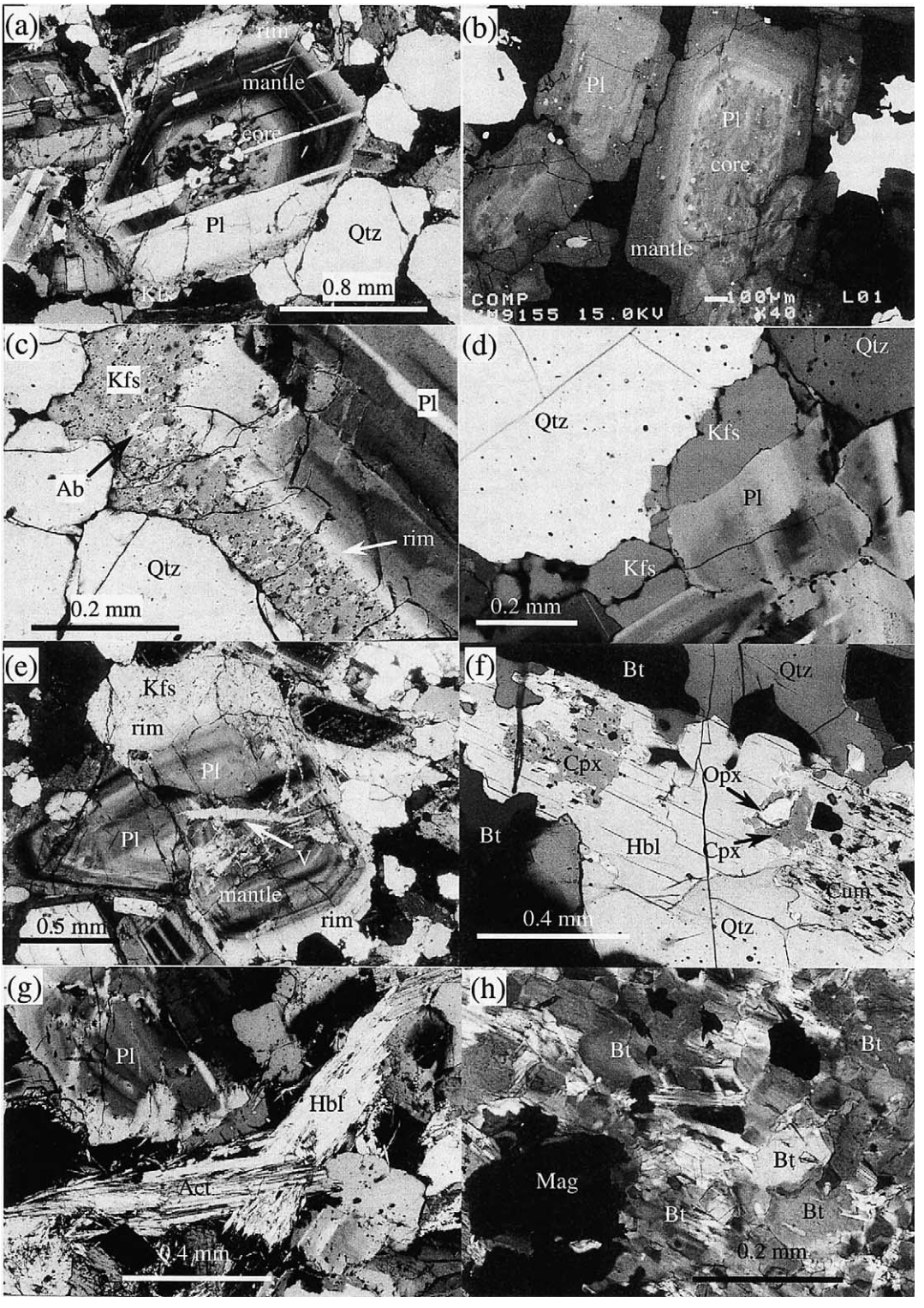
(a)
rim
mantle
core
Pl
Qtz
Kfs
0.8 mm
(b)
Pl
Pl
core
mantle
COMP
M9155 15.0KV
100μm
X40
L01
(c)
Kfs
Pl
Ab
rim
Qtz
0.2 mm
(d)
Qtz
Qtz
Kfs
Pl
Kfs
0.2 mm
(e)
Kfs
rim
Pl
Pl
V
mantle
0.5 mm
rim
(f)
Bt
Qtz
Cpx
Opx
Bt
Hbl
Cpx
Cum
0.4 mm
Qtz
(g)
Pl
Hbl
Act
0.4 mm
(h)
Bt
Bt
Bt
Mag
Bt
Bt
0.2 mm

rounded by clinopyroxene or altered to cummingtonite in C13 (Fig. 4f). Actinolite sporadically occurs as parts of coarse hornblende in the samples and around microfractures within coarse hornblende in C11 and C12. Fluid inclusions sometimes align along the microfractures. Actinolite as fibrous grains occurs in coarse hornblende (Fig. 4g) and with titanite along fractured parts of rocks in C11. Biotite occurs as coarse platy grains and fine flaky grains in C11 and C12 (Fig. 4h). Magnetite is frequently included in hornblende and biotite of the samples and exhibits exsolution lamellae of ilmenite with widths less than 10 μm in C13.

Free interstitial spaces are identified in C13: euhedral biotite facing the free interstitial space (Fig. 4k), plagioclase, K-feldspar and quartz with rounded surfaces surrounding the free interstitial space (Fig. 4l) and plagioclase with sharp surfaces surrounding the free interstitial spaces (Fig. 4m). The euhedral biotite is most reliable to clarify the presence of free interstitial spaces in C13.

4. Mineral chemistry

Chemical compositions of minerals were analyzed using an electron probe microanalyzer (EPMA: JEOL JXA 8800R) at the Geological Survey of Japan (GSJ). The analytical conditions were: acceleration voltage of 15 kV, current emission of 1.2×10^{-8} A and counting time of 20 s. The correction method was after Bence and Albee (1968).

Plagioclase chemistry is characterized by variations of An_{85-2} in C11, An_{92-10} in C12, and An_{87-24} in C13 (Fig. 5A). Anorthite contents at the cores of plagioclase without patchy zoning are 92–69 mol%, and those at the most marginal parts of mantles are about 20 mol% in C11 and C12 and 24 mol% in C13. Orthoclase contents of pla-

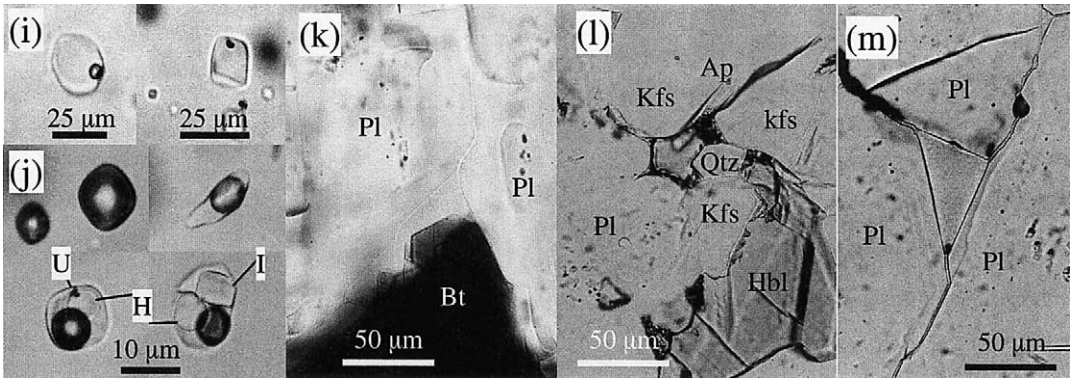

Fig. 4 (*Continued*). Photomicrographs of the Kakkonda Granite. (a) Plagioclase consists of an irregularly shaped core with patchy zoning and a mantle with oscillatory zoning that is surrounded by albite-rich rims (C11). Crossed nicols. (b) Plagioclase consists of an irregularly shaped core with patchy zoning and a mantle with oscillatory zoning without a rim (C13). SEM image. (c) Interstitial K-feldspar exhibits perthite by exsolution of albite lamella (C11). Crossed nicols. (d) Interstitial K-feldspar exhibits no perthite and contacts plagioclase with sharp surfaces (C13). Crossed nicols. (e) Sealed microfracture is composed of oligoclase (shown as 'V') and occurs in plagioclase (C12). Crossed nicols. (f) Hornblende includes orthopyroxene, clinopyroxene and cummingtonite, in which orthopyroxene is surrounded by clinopyroxene (C13). Crossed nicols. (g) Fibrous actinolite occurs within coarse hornblende (C11). Crossed nicols. (h) Fine flaky biotite occurs as an aggregate within coarse biotite (C12). Crossed nicols. (i) Quartz of C13 includes glassy melt inclusions, which have spherical shapes (left) or negative crystal shapes of β-quartz (right). One nicol. (j) Quartz in the samples contains various types of fluid inclusions: vapor-rich two-phase inclusion (left-top), liquid-rich two-phase inclusion (right-top) and polyphase inclusion (bottom). The liquid-rich inclusion occurs in C11 and C12 and vapor-rich and polyphase inclusions occur in all three samples. Abbreviations: H, halite; I, iron-bearing chloride; U, unidentified mineral. One nicol. (k) Euhedral biotite faces the interstitial space (C13). One nicol. (l) The interstitial space is surrounded by plagioclase, K-feldspar and quartz with rounded surfaces (C13). One nicol. (m) The interstitial space is surrounded by plagioclase with sharp surfaces (C13). One nicol. Abbreviations: Ab, albite; Ap, apatite; Bt, biotite; Cpx, clinopyroxene; Cum, cummingtonite; Hbl, hornblende; Kfs, K-feldspar; Mag, magnetite; Opx, orthopyroxene; Pl, plagioclase; Qtz, quartz.

gioclase increase to 3 mol% as the An contents decrease to about 25 mol%. Below this value, Or contents decrease to 1 mol% in C11 and scatter within 1–4 mol% in C12. The sealed microfractures observed in C11 and C12 are composed of oligoclase ($Ab_{77-87}An_{23-13}$).

Interstitial K-feldspar has Ab contents of 7–13 mol% in C11, 9–11 mol% in C12 and 14–17 mol% in C13 with An contents less than 0.5 mol% in the samples (Table 2). Albite lamellae in K-feldspar have An contents of 1–6 mol% in C11 and more varied An contents of 2–18 mol% in C12 (Table 2). Anorthite contents in albite lamellae show a systematic increase from C11 through C12 toward the most marginal parts of plagioclase in C13 (Table 2; Fig. 5B).

Orthopyroxene has molecule ratios of $En_{46}Fs_{52}Wo_2$–$En_{56}Fs_{42}Wo_2$, and clinopyroxene, $En_{31}Fs_{20}Wo_{49}$–$En_{41}Fs_{15}Wo_{44}$ (Table 3; Fig. 5C). The orthopyroxene in the samples is relatively poor in En component compared to orthopyroxene in basic clots of granitic rocks collected from other deep cores ($En_{69}Fs_{30}Wo_1$–$En_{78}Fs_{21}Wo_1$; Kanisawa et al., 1994; Fig. 5C).

Hornblende is identified as magnesiohornblende to actinolite based on the classification of Leake et al. (1997) (Fig. 5D). Coarse hornblende has variations in mg-value (molecule ratio of Mg/(Mg+Fe+Mn)) of 0.52–0.79 in C11, 0.53–0.61 in C12 and 0.50–0.58 in C13 (Table 4). Fibrous actinolite in C11 has mg-values of 0.65–0.77, and actinolitic parts in coarse hornblende of C13 have mg-values of 0.56–0.68 (Table 4). Chemical compositions of hornblende in the samples are almost concordant to those of hornblende in granitic rocks from other deep cores (Kanisawa et al., 1994), with the exception of no magnesiohornblende with high mg-values in the studied samples (Fig. 5D). Cummingtonite in C13 has mg-values of 0.50–0.58 (Table 4).

Coarse platy biotite in C13 has the lowest mg-values and Si contents among the Kakkonda granitic rocks (Table 5; Fig. 5E). Platy biotite in C11 and C12 shows slightly increasing mg-values with increasing Si contents. Flaky biotite might have relatively low mg-values and Si contents compared to platy biotite in C11 and C12 (Fig. 5E).

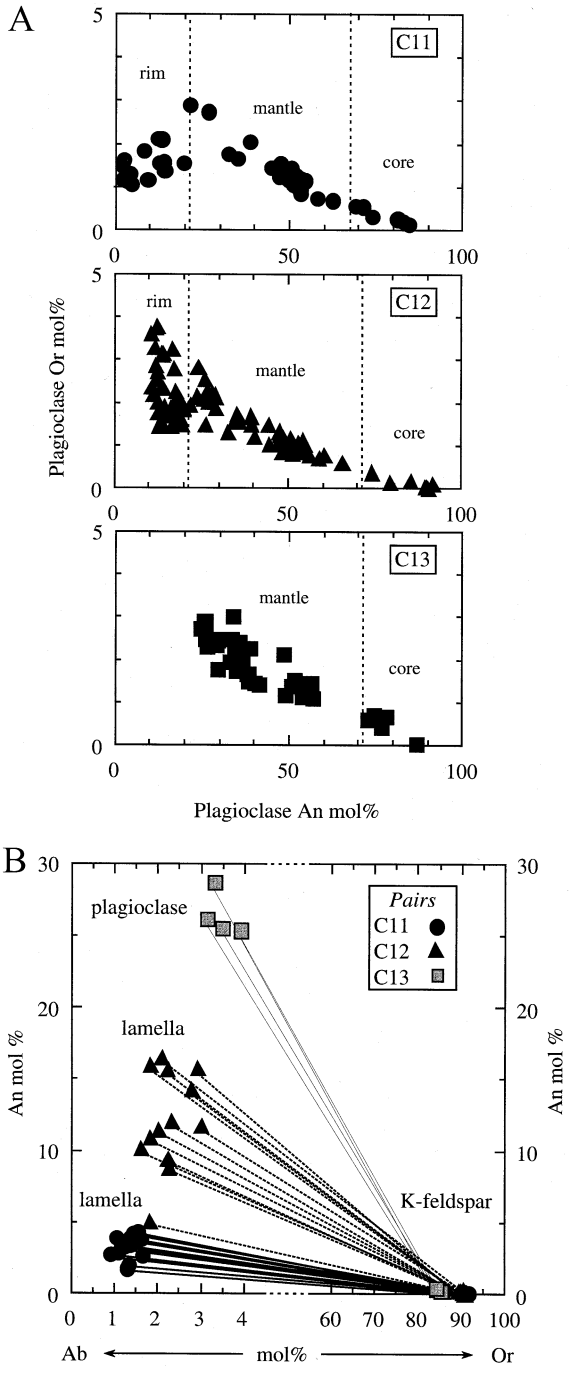

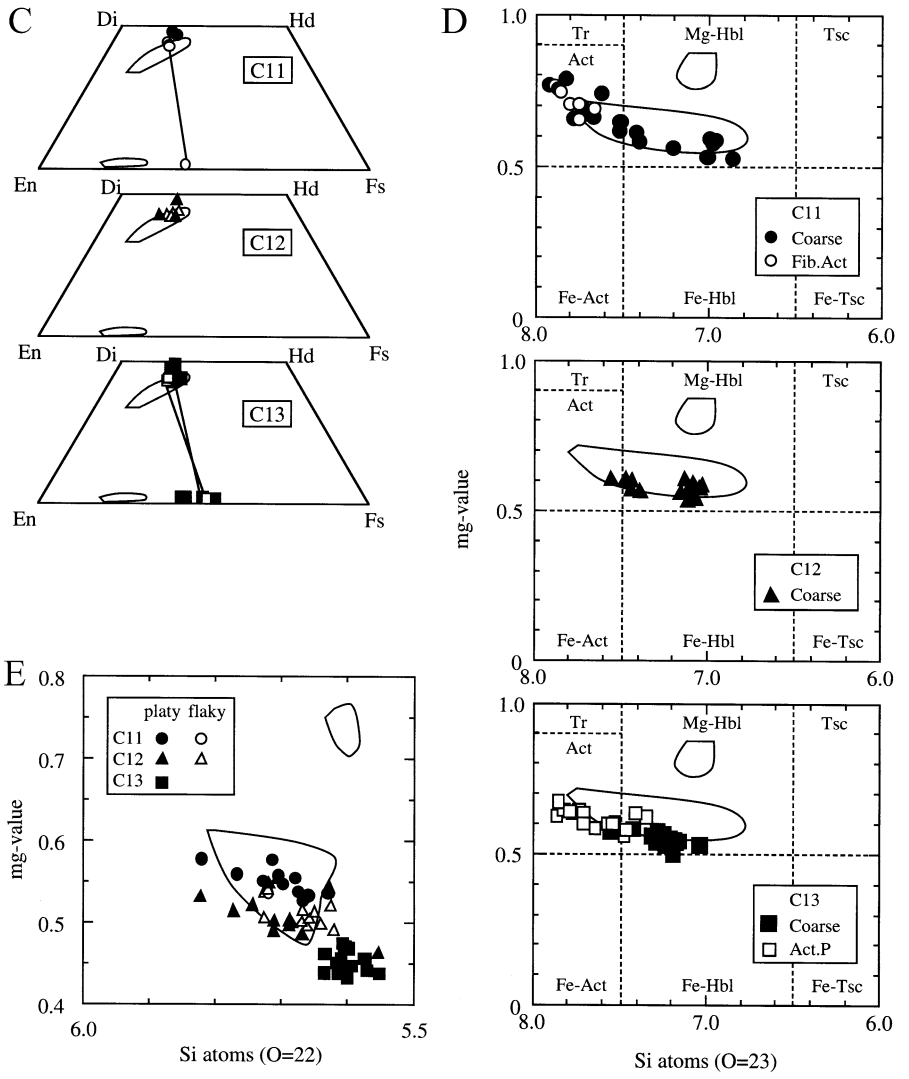

Fig. 5 (*Continued*). Mineral chemistry of the Kakkonda Granite. (A) Anorthite (An) and orthoclase (Or) contents of plagioclase. (B) Molecule ratios of anorthite (An), albite (Ab) and orthoclase (Or) for pairs of K-feldspar and its albite lamella in C11 and C12 compared to the ratios for pairs of K-feldspar and most marginal parts of plagioclase adjacent to the K-feldspar in C13. (C) Molecule En–Fs–Wo ratios of pyroxene. Abbreviations: Di, diopside; En, enstatite; Fs, ferrosilite; Hd, hedenbergite; Wo, wollastonite; solid symbols, pyroxene in hornblende; open symbols, pyroxene in plagioclase; closed curves, range of pyroxene in granitic rocks collected from other deep cores (Kanisawa et al., 1994). (D) Hornblende Si contents and mg-values projected on a diagram of Leake et al. (1997). Abbreviations: Coarse, coarse grain; Fib.Act, actinolite as fibrous grain; Act.P, actinolitic part in coarse hornblende; mg-value, molecule ratio of Mg/(Mg+Fe+Mn); Act, actinolite; Fe-Act, ferroactinolite; Mg-Hbl, magnesio-hornblende; Fe-Hbl, ferrohornblende; Tr, tremolite; Tsc, tschermakite; Fe-Tsc, ferrotschermakite; closed curves, range of hornblende in granitic rocks collected from other deep cores (Kanisawa et al., 1994). (E) Biotite Si contents and mg-values. Abbreviations: mg-value, molecular ratio of Mg/(Mg+Fe+Mn); closed curves, range for biotite in granitic rocks collected from other deep cores (Kanisawa et al., 1994).

Table 2
Molecule ratios of pairs of K-feldspar and its albite lamella in C11 and C12 and pairs of K-feldspar and marginal parts of plagioclase adjacent to the K-feldspar in C13 (listed in descending order of An contents in albite lamella and plagioclase)

Core name (MPa)[a]	Albite lamella (mol%)			K-feldspar (mol%)			(°C)[b]		
	Ab	Or	An	Ab	Or	An	T_{Or}	T_{Ab}	T_{An}
C11 (0.73)	94.3	1.4	4.3	9.6	90.4	0.0	354	347	
	94.5	1.3	4.2	9.1	90.8	0.1	346	336	1036
	95.1	1.0	3.9	9.2	90.7	0.1	315	337	986
	94.7	1.5	3.8	8.6	91.4	0.0	356	329	
	94.9	1.3	3.8	9.8	90.2	0.0	344	348	
	95.4	1.1	3.5	10.1	89.7	0.2	324	349	1304
	95.4	1.3	3.3	8.7	91.3	0.0	335	329	
	95.7	1.1	3.2	8.6	91.3	0.1	324	325	1147
	96.2	1.0	2.8	10.3	89.6	0.1	313	351	1172
	96.4	0.9	2.7	8.8	91.2	0.0	294	328	
	95.8	1.6	2.6	9.7	90.3	0.0	352	344	
	96.7	1.3	2.0	9.9	90.0	0.1	327	343	1404
	97.1	1.2	1.7	9.0	91.0	0.0	321	330	
C12 (0.81)	81.7	1.7	16.5	9.7	90.0	0.3	443	385	753
	82.6	1.5	15.9	9.6	90.4	0.0	424	384	
	81.8	2.4	15.7	11.0	88.9	0.2	484	407	668
	82.5	1.8	15.6	10.0	89.9	0.1	448	390	526
	83.4	2.3	14.2	9.5	90.4	0.0	469	379	
	86.0	2.0	12.0	10.0	89.9	0.1	438	377	628
	85.7	2.6	11.7	9.3	90.7	0.1	468	366	586
	86.9	1.8	11.3	9.6	90.3	0.1	422	367	712
	87.5	1.6	10.9	10.5	89.3	0.2	407	379	768
	88.4	1.4	10.1	10.5	89.3	0.2	390	375	869
	88.6	2.0	9.4	11.0	88.9	0.2	423	382	828
	89.2	2.0	8.8	9.4	90.6	0.0	420	358	
	93.3	1.7	5.0	9.3	90.7	0.1	375	344	805

Core name (MPa)[a]	Plagioclase (mol%)			K-feldspar (mol%)			(°C)[b]		
	Ab	Or	An	Ab	Or	An	T_{or}	T_{ab}	T_{an}
C13 (0.93)	69.1	2.3	28.6	14.7	85.1	0.2	543	530	512
	71.7	2.3	26.1	15.9	83.8	0.3	532	534	599
	71.9	2.6	25.5	14.9	84.9	0.2	546	518	550
	71.8	2.9	25.3	16.2	83.4	0.4	564	535	666

[a] Lithostatic pressures at the sampling depths under the assumtion of a rock density of 2.5 g/cm^3.
[b] Equilibrium temperatures for Or, Ab and An components of the pairs (T_{Or}, T_{Ab} and T_{An}, respectively) calculated through the two-feldspar geothermoeter of Fuhrman and Lindsley (1988).

Magnetite has mole fractions of ulvöspinel component (X_{Usp}) less than 0.004 in C11, 0.056 in C12 and 0.060–0.069 in C13 (Table 6). Ilmenite lamella in magnetite of C13 has mole fractions of ilmenite component (X_{Ilm}) of 0.946–0.967 (Table 6).

5. Melt inclusion

Melt inclusions in plagioclase were all devitrified, and the devitrification made the inclusions unsuitable for analysis. Melt inclusions in quartz of C13 are not devitrified, and chemical compositions of the glass phase were analyzed using EPMA at GSJ with analytical conditions of an acceleration voltage of 15 kV, a current emission of 1.2×10^{-9} A and a counting time of 6 s. The correction method was after Bence and Albee (1968).

The glass phase of melt inclusions in quartz has

Table 3
Representative chemical compositions of pyroxene

Core name	C11				C12		C13			
Mineral Host[d]	Cpx (pl)	Cpx (hbl)	Cpx[a] (pl)	Opx[a] (pl)	Cpx (pl)	Cpx (hbl)	Cpx[b] (hbl)	Opx[b] (hbl)	Cpx[c] (pl)	Opx[c] (pl)
SiO_2 (wt%)	51.59	52.34	51.04	49.81	52.71	52.71	52.18	51.54	52.23	50.63
TiO_2	0.27	0.06	0.19	0.14	0.05	0.00	0.11	0.08	0.20	0.15
Al_2O_3	1.06	0.19	0.96	0.55	0.50	0.24	0.47	0.31	0.99	0.58
Cr_2O_3	0.00	0.00	0.01	0.01	0.03	0.08	0.00	0.00	0.01	0.03
FeO[e]	10.86	11.40	11.45	27.10	12.74	11.25	12.30	28.96	10.55	30.39
MnO	0.45	0.60	0.52	1.11	0.91	0.75	0.64	1.49	0.50	1.22
MgO	13.43	11.95	13.80	18.94	11.88	11.53	12.80	16.54	13.43	16.50
CaO	21.48	23.35	21.87	1.10	21.85	24.09	21.81	1.14	21.83	0.99
Na_2O	0.26	0.20	0.24	0.01	0.30	0.22	0.22	0.01	0.27	0.01
K_2O	0.00	0.00	0.00	0.00	0.01	0.00	0.00	0.00	0.00	0.00
Total	99.41	100.9	100.09	98.76	100.97	100.87	100.52	100.06	100.01	100.50
O = 6										
Si	1.956	1.985	1.934	1.943	1.986	1.987	1.971	1.994	1.966	1.964
Ti	0.008	0.002	0.006	0.004	0.001	0.000	0.003	0.002	0.006	0.004
Al	0.048	0.009	0.043	0.025	0.022	0.011	0.021	0.014	0.044	0.027
Cr	0.000	0.000	0.000	0.000	0.001	0.002	0.000	0.000	0.000	0.001
Fe	0.344	0.362	0.363	0.884	0.401	0.355	0.389	0.937	0.332	0.986
Mn	0.014	0.019	0.017	0.037	0.029	0.024	0.020	0.049	0.016	0.040
Mg	0.759	0.676	0.779	1.101	0.667	0.648	0.721	0.954	0.754	0.954
Ca	0.873	0.949	0.888	0.046	0.882	0.973	0.883	0.047	0.880	0.041
Na	0.019	0.015	0.018	0.001	0.022	0.016	0.016	0.000	0.020	0.001
K	0.000	0.000	0.000	0.000	0.000	0.000	0.000	0.000	0.000	0.000
Total	4.022	4.016	4.048	4.041	4.012	4.015	4.023	3.997	4.017	4.018
En (%)	38.4	34.0	38.4	54.2	34.2	32.8	36.2	49.2	38.3	48.2
Fs	17.4	18.2	17.9	43.5	20.6	17.9	19.5	48.4	16.9	49.8
Wo	44.2	47.8	43.7	2.3	45.2	49.3	44.3	2.4	44.8	2.1
T (°C)[f]	831						822		838	

[a] Included in the same grain.
[b] Included in the same grain.
[c] Included in the same grain.
[d] (hbl), surrounded by hornblende; (pl), included in a core of plagioclase.
[e] Total iron as Fe^{2+}.
[f] Equilibrium temperatures calculated through the two-pyroxene geothermometer of Wood and Banno (1973).

a chemical composition approximated to the quaternary $NaAlSi_3O_8$–$KAlSi_3O_8$–SiO_2–H_2O system (Table 7; Fig. 6). The norm Ab to Or ratios of the melt inclusions are from 0.91 to 0.97. The melt inclusions probably contain volatiles of several weight percent because the totals of major oxides are about 95 wt%. Sulfur and chlorine contents were below the detection limits of EPMA under the studied conditions.

Microthermometry of the melt inclusions was conducted using a Leitz 1350 heating stage at GSJ. The uncertainty of the measurement is within ±10°C at 700°C. During heating, bubbles appear in the melt inclusions at 540–610°C and homogenize into the glass phase at 710–750°C.

6. Geothermometry

Geothermometers as described in the following publications were applied to the samples: the two-pyroxene geothermometer of Wood and Banno (1973), the hornblende–plagioclase geothermometer of Holland and Blundy (1994), the magnetite–

Table 4
Representative chemical compositions of hornblende

Core name	C11			C12		C13			C13
Mineral[a]	Hbl C	Hbl C	Act F	Hbl C	Hbl C	Hbl C	Hbl C	Act C	Cum (Hbl)
SiO_2 (wt%)	47.10	50.11	55.34	47.08	50.37	46.53	49.13	52.79	52.63
TiO_2	1.55	0.87	0.22	1.50	0.69	1.03	0.71	0.11	0.08
Al_2O_3	6.73	3.67	1.02	6.14	3.90	5.97	5.35	2.18	1.61
Cr_2O_3	0.00	0.00	0.00	0.03	0.00	0.02	0.00	0.00	0.00
FeO[b]	15.85	16.94	10.05	16.40	16.89	18.39	17.62	14.69	23.88
MnO	0.35	0.57	0.17	0.36	0.63	0.54	0.58	0.68	1.50
MgO	13.17	13.78	17.97	12.85	13.14	11.96	12.58	15.06	14.66
CaO	10.85	10.54	12.23	10.69	10.89	10.78	11.28	11.39	3.30
Na_2O	1.66	1.14	0.55	1.69	0.96	1.30	0.96	0.34	0.22
K_2O	0.33	0.41	0.19	0.37	0.30	0.68	0.48	0.11	0.08
Total	97.60	98.02	97.73	97.10	97.76	97.21	98.69	97.35	97.96
O = 23									
Si	6.987	7.394	7.862	7.040	7.440	7.036	7.239	7.708	7.804
Ti	0.173	0.097	0.023	0.169	0.076	0.117	0.079	0.013	0.009
Al	1.177	0.638	0.170	1.082	0.679	1.064	0.929	0.375	0.281
Cr	0.000	0.000	0.000	0.003	0.000	0.003	0.000	0.000	0.000
Fe	1.966	2.090	1.194	2.052	2.086	2.326	2.172	1.793	2.961
Mn	0.044	0.071	0.020	0.045	0.079	0.069	0.073	0.084	0.189
Mg	2.911	3.032	3.805	2.865	2.894	2.696	2.763	3.278	3.240
Ca	1.724	1.666	1.862	1.713	1.723	1.747	1.780	1.782	0.524
Na	0.479	0.325	0.152	0.489	0.274	0.380	0.273	0.097	0.062
K	0.063	0.076	0.034	0.071	0.057	0.131	0.091	0.021	0.014
Total	15.523	15.390	15.123	15.528	15.309	15.569	15.400	15.151	15.085
mg-value	0.592	0.584	0.758	0.577	0.572	0.530	0.552	0.636	0.507
f[c]	0.9900	0.9980	0.9980	0.9925	0.9926	0.9919	0.9887	0.9946	
P (kb)[d]	0.73	0.73	0.73	0.81	0.81	0.93	0.93	0.93	
Pl (An%)[e]	20	20	5	20	20	25	25	25	
T (°C)[f]	771	694	504	764	661	774	698	553	

[a] Hbl, hornblende; Act, actinolite; Cum, cummingtonite; C, coarse grain; F, fibrous grain; (Hbl), in hornblende.
[b] Total iron as Fe^{2+}, mg-value: molecule ratio of Mg/(Mg+Fe+Mn).
[c] Normalization factor to calculate ferric iron content by the method of Holland and Blundy (1994).
[d] Lithostatic pressure at the sampling depths using a rock density of 2.5 g/cm^3.
[e] Anorthite molecule content at a part in plagioclase assumed to be crystallized with hornblende.
[f] Equilibrium temperatures determined from the hornblende–plagioclase geothermometer of Holland and Blundy (1994).

ilmenite geothermometer of Anderson and Lindsley (1988) and the two-feldspar geothermometer of Fuhrman and Lindsley (1988). In the application, total pressures were assumed to be equal to the lithostatic fluid pressures at the sampling depths under the assumption of a rock density of 2.5 g/cm^3.

The Wood and Banno geothermometer was applied to the orthopyroxene and clinopyroxene pairs included at the cores of plagioclase in C11 and C13 and indicated equilibrium temperatures of 831° and 838°C within an accuracy of ±70°C, respectively (Table 3). A pair of orthopyroxene and clinopyroxene that surrounds the orthopyroxene in C13 indicates an equilibrium temperature of 822°C (Table 3). These three temperatures are concordant with the temperatures reported for orthopyroxene–clinopyroxene pairs in basic clots of granitic rocks collected from other deep cores (869–874°C: Kanisawa et al., 1994).

In the application of the Holland and Blundy geothermometer, whose uncertainty is within

Table 5
Representative chemical compositions of biotite

Core name	C11			C12			C13
	P[a]	P	F[b]	P	P	F	P
SiO_2 (wt%)	38.49	37.38	37.90	37.77	37.18	37.84	36.31
TiO_2	3.24	4.54	4.03	3.26	3.54	3.63	3.60
Al_2O_3	12.43	12.89	12.46	13.37	13.18	13.32	13.05
Cr_2O_3	0.03	0.00	0.00	0.00	0.00	0.00	0.01
FeO[c]	17.28	18.46	19.37	18.26	20.90	18.40	22.58
MnO	0.36	0.26	0.25	0.37	0.44	0.42	0.38
MgO	13.50	12.18	12.68	12.69	11.31	12.42	10.04
CaO	0.03	0.06	0.01	0.00	0.04	0.00	0.00
Na_2O	0.10	0.12	0.10	0.10	0.07	0.11	0.17
K_2O	10.43	10.30	10.15	10.37	10.20	10.19	9.90
Total	95.88	96.18	96.96	96.20	96.84	96.32	96.04
O = 22							
Si	5.819	5.674	5.719	5.719	5.668	5.720	5.635
Ti	0.369	0.518	0.458	0.371	0.406	0.412	0.420
Al	2.214	2.306	2.217	2.386	2.368	2.372	2.387
Cr	0.003	0.000	0.000	0.000	0.000	0.000	0.002
Fe	2.185	2.343	2.444	2.312	2.665	2.326	2.931
Mn	0.046	0.033	0.032	0.048	0.057	0.053	0.050
Mg	3.042	2.756	2.851	2.865	2.570	2.799	2.323
Ca	0.005	0.009	0.002	0.000	0.006	0.000	0.000
Na	0.029	0.035	0.030	0.029	0.020	0.031	0.050
K	2.013	1.995	1.954	2.004	1.984	1.965	1.960
Total	15.724	15.670	15.707	15.733	15.744	15.680	15.756
mg-value[d]	0.577	0.537	0.535	0.548	0.486	0.540	0.438

[a] P, platy grain.
[b] F, flaky grain.
[c] Total iron as Fe^{2+}.
[d] Molecule ratio of Mg/(Mg+Fe+Mn).

±75°C, coarse hornblende was assumed to be crystallized with the most marginal parts at mantles of plagioclase (An_{20} for C11 and C12 and An_{25} for C13; Table 4). The assumption presents minimum crystallization temperatures for at least the coarse hornblende in C13. The pairs of coarse hornblende and plagioclase indicate the crystallization of coarse hornblende at 640–780°C in C11, 650–770°C in C12 and 690–720°C in C13 most frequently (Table 4; Fig. 7a). Actinolitic parts in coarse hornblende of C13 were also assumed to be equilibrated with the most marginal parts at mantles of plagioclase (An_{25}; Table 4). The pairs indicate equilibrium temperatures of 470–650°C (Table 4), which are almost above the logged temperatures (Fig. 7a). Fibrous actinolite in C11 was assumed to be equilibrated with rims of plagioclase (An_5; Table 4). The pairs indicate equilibrium temperatures of 450–540°C (Table 4; Fig. 7a).

The Anderson and Lindsley geothermometer indicates equilibrium temperatures of 520–590°C for pairs of magnetite and its ilmenite lamella in C13 within an error of ±5°C (Table 6).

The Fuhrman and Lindsley geothermometer can calculate an equilibrium temperature for each Ab, Or and An component between pairs of plagioclase and K-feldspar (T_{Ab}, T_{Or} and T_{An}, respectively) within an uncertainty of ±40°C over 650°C, in which each temperature is defined as a function of six molecule ratios (X^{Pl}_{Ab}, X^{Pl}_{or}, X^{Pl}_{An}, X^{Kfs}_{Ab}, X^{Kfs}_{or} and X^{Kfs}_{An}). In the calculation, T_{Ab} is the most sensitive to the Ab content in K-feldspar, and T_{Or} is the most sensitive to the Or content in plagioclase (Fuhrman and Lindsley,

Table 6
Representative chemical compositions of magnetite and its ilmenite lamella

Core name	C11		C12	C13			
Mineral[a]	Mag	Mag	Mag	Mag[b]	Ilm[b]	Mag[c]	Ilm[c]
SiO_2 (wt%)	0.03	0.12	0.03	0.03	0.01	0.05	0.05
TiO_2	0.14	0.03	1.93	2.05	49.15	2.11	49.16
Al_2O_3	0.11	0.09	0.07	0.45	0.02	0.44	0.01
Cr_2O_3	0.00	0.07	0.12	0.12	0.01	0.08	0.04
FeO[d]	91.15	92.55	92.04	88.94	47.20	88.70	48.61
MnO	0.13	0.15	0.38	0.36	2.38	0.42	2.28
MgO	0.03	0.06	0.07	0.13	0.53	0.11	0.54
CaO	0.06	0.01	0.02	0.00	0.00	0.00	0.01
Na_2O	0.00	0.00	0.01	0.00	0.02	0.04	0.00
K_2O	0.00	0.00	0.02	0.01	0.01	0.01	0.01
Total	91.64	93.09	94.69	92.09	99.33	91.95	100.71
Oxygen	4	4	4	4	3	4	3
Si	0.001	0.005	0.001	0.001	0.000	0.002	0.001
Ti	0.004	0.001	0.055	0.060	0.932	0.062	0.919
Al	0.005	0.004	0.003	0.021	0.001	0.020	0.000
Cr	0.000	0.002	0.003	0.004	0.000	0.003	0.001
Fe^{3+}	1.985	1.982	1.883	1.854	0.136	1.854	0.159
Fe^{2+}	0.996	0.997	1.036	1.041	0.859	1.037	0.852
Mn	0.004	0.005	0.012	0.012	0.051	0.014	0.048
Mg	0.002	0.004	0.004	0.007	0.020	0.006	0.020
Ca	0.003	0.000	0.001	0.000	0.000	0.000	0.000
Na	0.000	0.000	0.001	0.000	0.001	0.003	0.000
K	0.000	0.000	0.001	0.000	0.000	0.000	0.000
Total	3.000	3.000	3.000	3.000	2.000	3.000	2.000
X_{Usp}[e]	0.004	0.001	0.056	0.061		0.063	
X_{Ilm}					0.967		0.953
T (°C)[f]				528		563	

[a] Mag, magnetite; Ilm, ilmenite.
[b] Included in the same grain.
[c] Included in the same grain.
[d] Total iron as Fe^{2+}.
[e] Usp, ulvöspinel.
[f] Calculated through the magnetite-ilmenite geothermometer of Anderson and Lindsley (1988).

1988). The geothermometer was applied to the pairs of K-feldspar and its albite lamella in C11 and indicated similar T_{Or} and T_{Ab} at 294–356°C with discordantly high T_{An} over 986°C (Table 2; Fig. 7b). Pairs of K-feldspar and its albite lamella in C12 indicate a relatively low T_{Ab} of 344–407°C and high T_{Or} of 375–484°C with discordantly high T_{An} over 526°C (Table 2; Fig. 7b). In C13, K-feldspar was assumed to be equilibrated with the most marginal parts of plagioclase. The pairs indicate concordant temperatures among T_{Or}, T_{Ab} and T_{An} at 512–564°C with the exception of two T_{An} at 599° and 666°C (Table 2; Fig. 7b). The discordantly high T_{An} in C11 and C12 could be attributed to the low An contents in the K-feldspar (Table 2).

The textural and mineralogical relations of the Kakkonda Granite have evolved as follows at the depth of C13 (Fig. 7c). The granitic magma began to be crystallized over 840°C, suspending the crystallized basic clots based on the temperatures determined from the two-pyroxene geothermometer (Fig. 7c). The crystallization temperatures of coarse hornblende determined from the hornblende–plagioclase geothermometer (mostly at 690–720°C) are almost concordant with the mea-

Table 7
Chemical compositions of melt inclusions in quartz

SiO_2 (wt%)	68.5 (2.7)	69.8 (2.8)	69.0 (2.3)
TiO_2	0.3 (0.2)	0.0 (–)	0.1 (0.2)
Al_2O_3	14.3 (1.2)	14.6 (1.2)	15.2 (1.4)
Cr_2O_3	0.0 (–)	0.0 (0.0)	0.0 (–)
FeO[a]	0.4 (0.3)	0.1 (0.1)	0.4 (–)
MnO	0.0 (–)	0.0 (–)	0.3 (0.4)
MgO	0.0 (–)	0.1 (0.2)	0.1 (0.1)
CaO	1.1 (0.4)	1.4 (0.5)	1.9 (0.7)
Na_2O	3.7 (1.0)	4.2 (1.0)	3.4 (0.9)
K_2O	5.8 (0.9)	6.5 (1.0)	5.0 (1.0)
Total	94.1	96.6	95.4
norm (wt%)			
Q	23.3	19.1	27.1
or	34.3	38.4	29.5
ab	31.3	35.5	28.8
an	3.2	2.1	5.5

In parentheses: statistical error.
[a] Total iron as Fe^{2+}.

sured homogenization temperatures of melt inclusions in quartz (710–750°C; Fig. 7c). Both temperatures are close to the solidification temperature of a hydrous granitic melt (e.g. 720°C at 100 MPa: Tuttle and Bowen, 1958). Thus, the granitic magma became to be solidified at 690–750°C. After crystallization of the magma, coarse hornblende is partly altered to actinolite in the range of 470–650°C (Fig. 7c). Magnetite exsolved ilmenite lamella in the range of 520–590°C (Fig. 7c). K-feldspar in C13 seems to be presently equilibrated with marginal parts of plagioclase at 512–564°C in all the Ab, Or and An components (Fig. 7c).

7. Petrographic features of the high-temperature granite

The Kakkonda Granite collected over 500°C (C13) possesses the following remarkable petrographic features in contrast to those collected at 410°C (C12) and 370°C (C11): (1) Interstitial spaces are not completely sealed; (2) K-feldspar exhibits no perthite; (3) quartz contains glassy melt inclusions without devitrification; (4) hornblende is less intensively altered to actinolite, and biotite is not altered.

7.1. Free interstitial spaces

Tuttle (1952) inferred that free interstitial spaces in granites could be sealed by precipitation of alteration minerals and plastic deformation of quartz during cooling of granites. However, free interstitial spaces still remain in C13 (Fig. 4k–m). The free interstitial spaces are considered to be filled with gas-rich fluids and hypersaline fluids (Ikeuchi et al., 1998; Kasai et al., 1998). The Kakkonda Granite has permeabilities by an order of magnitude higher than various granites such as the Westery, Inada and Takidani granites (Fujimoto et al., 2000). The free interstitial spaces observed in this study might contribute to the high permeability, possibly in C13.

7.2. Absence of perthite in K-feldspar

Tuttle (1952) and Tuttle and Bowen (1958) suggested that perthite in K-feldspar is a recrystallization texture formed during the cooling of granites. This study directly produces the evidence;

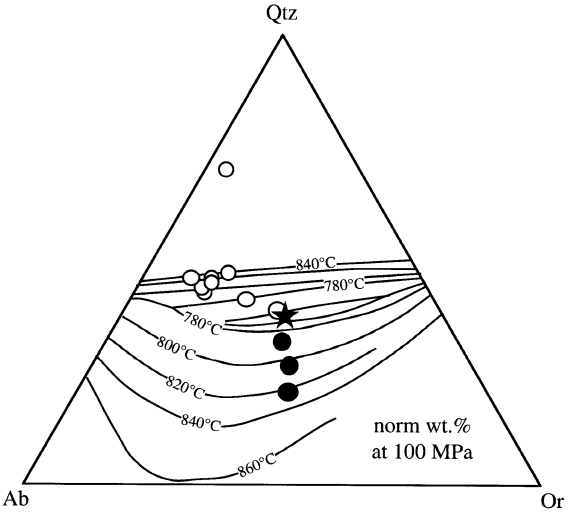

Fig. 6. Norm Qtz–Ab–Or ratios of melt inclusions in quartz of C13 (solid symbol) projected on a diagram of the hydrous Qtz–Ab–Or system of Tuttle and Bowen (1958). Open symbols indicate norm Qtz–Ab–Or ratios in the bulk composition of granitic rocks from other deep cores (data after Kanisawa et al., 1994), and star symbol indicates the norm Qtz–Ab–Or ratio at the ternary minimum (about $Qtz_{40}Ab_{30}Or_{30}$: Tuttle and Bowen, 1958).

K-feldspar exhibits perthite at 370–410°C in C11 and C12 (Fig. 4c), but not over 500°C in C13 (Fig. 4d). The formation of perthite in K-feldspar is considered to be related to the fluid composition as well as temperature. Lagache and Weisbrod (1977) found that two alkali feldspars could coexist with a fluid that has a K/Na mole ratio of 0.2 at 500°C and 100 MPa in experiments of the $NaAlSi_3O_8$–$KAlSi_3O_8$–NaCl–KCl–H_2O system. The hypersaline fluid obtained from the bottom level of well WD-1a has a K/Na mole ratio of 0.37 (Kasai et al., 1998). Therefore, K-feldspar in C13 does not form perthite when soaked in a fluid with such a high K/Na mole ratio.

The diffusion coefficients of Na in K-feldspar and K in albite at 500°C have been experimentally determined to be from 10^{-15} to 10^{-17} cm^2/s and from 10^{-19} to 10^{-20} cm^2/s, respectively, under wet to dry conditions (Smith, 1974; Giletti and Shanahan, 1997). It takes 0.03 million years to diffuse

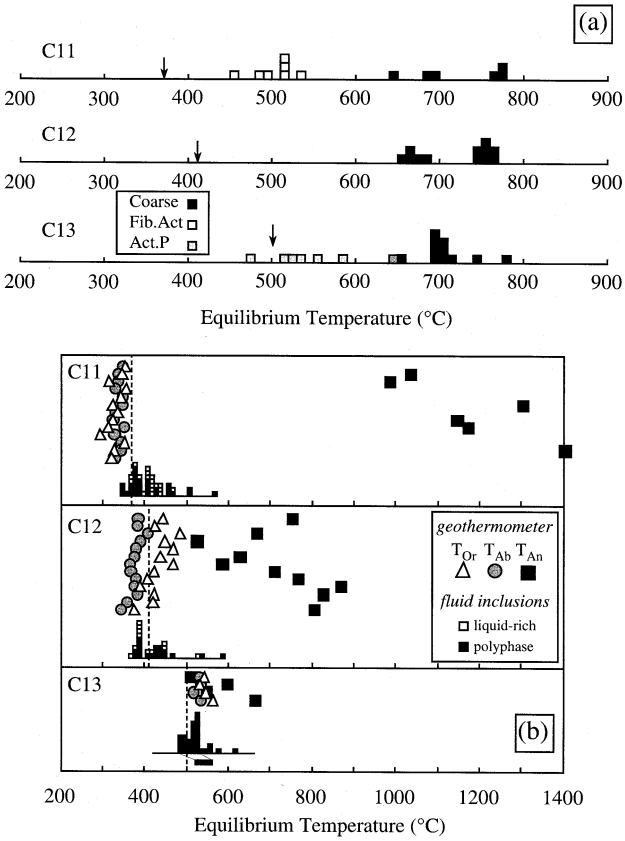

Fig. 7. Temperatures determined from geothermometers in publications. (a) Temperatures determined from the hornblende–plagioclase geothermometer of Holland and Blundy (1994). Vertical arrows indicate the logged temperatures at the sampling depths after Ikeuchi et al. (1998). Abbreviations are the same as in Fig. 5D. (b) Equilibrium temperatures of Ab, Or and An components between pairs of K-feldspar and plagioclase (T_{Ab}, T_{Or}, T_{An}, respectively) determined from the two-feldspar geothermometer of Fuhrman and Lindsley (1988). Dotted lines indicate the logged temperatures at the sampling depths after Ikeuchi et al. (1998), and homogenization temperatures of liquid-rich and polyphase fluid inclusions are after Komatsu et al. (1998). A thick bar drawn underneath the histogram of homogenization temperatures for C13 indicates trapping temperatures of fluid inclusions calculated with a fluid pressure correction up to the lithostatic pressure at the sampling depth (93 MPa). (c) A summary of various temperatures obtained for C13. The logged temperatures are after Ikeuchi et al. (1998), and homogenization temperatures of fluid inclusions are after Komatsu et al. (1998). The vertical hatched area indicates the range of solidification temperatures of the Kakkonda Granite. The thick bar drawn underneath the histogram of homogenization temperatures of fluid inclusions is the same as in Fig. 7b.

Na element for a distance of 0.1 mm in K-feldspar at a diffusion coefficient of 10^{-15} cm^2/s. The K-feldspar in C13 is less than 0.2 mm in width (Fig. 4d). Therefore, the K-feldspar in C13 could be homogeneous in composition and fully equilibrated with fluids in the interstitial spaces at an in situ temperature of over 500°C in the geological time span.

7.3. Undevitrified melt inclusions

Tuttle (1952) and Roedder (1992) suggested that glassy melt inclusions in quartz of granites are rare due to their elimination through recrystallization or are wholly crystallized during the cooling of granites. Conversely, glassy melt inclusions occurring in quartz without devitrification might be a feature of the high-temperature granite; the glassy melt inclusions are found in quartz of C13 (Table 1; Fig. 4i). The melt inclusions in C13 possibly contain volatiles of several weight percent, because the totals of major oxides are about 95 wt% (Table 7). The volatiles might prevent devitrification of the melt inclusions even below the solidification temperature of a hydrous granitic melt (e.g. 720°C at 100 MPa: Tuttle and Bowen, 1958).

The melt inclusions in C13 appear to be depleted in norm quartz in comparison to a melt at the ternary minimum of the hydrous Qtz–Ab–Or system (Fig. 6). The depletion of norm quartz could be attributed to the deposition of silica on the inclusion walls as quartz after trapping. Such depletion of silica has been generally identified in recrystallized melt inclusions (e.g. Frezzotti, 1992 for Mount Genis granite). The depletion of silica

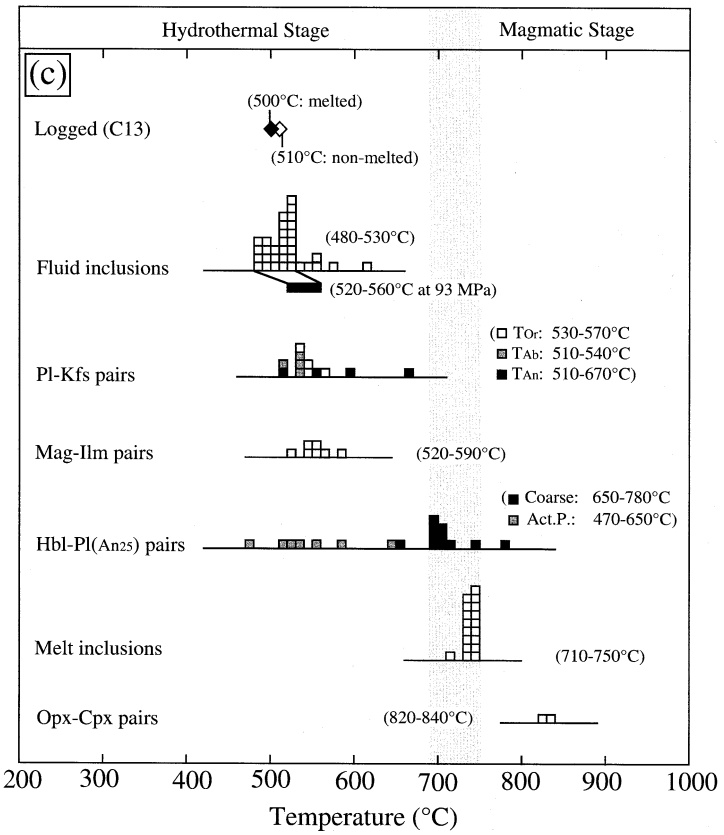

Fig. 7 (*Continued*).

might make homogenization temperatures of the studied melt inclusions higher than the true trapping temperatures (Fig. 7c).

The alkali ratios of melt inclusions in quartz are possibly considered not to be changed after the trapping. The Ab to Or ratios of the studied melt inclusions are almost concordant to the melt at the ternary minimum (Fig. 6). The melt inclusions are relatively rich in Or component in comparison to the bulk compositions of the granitic rocks from other deep cores (Fig. 6). A rock that has the most similar alkali ratio to the melt inclusions in Fig. 6 is a leucocratic granitic rock of Kanisawa et al. (1994), which has the highest Si content (75 wt%) among the Kakkonda granitic rocks. Therefore, the melt inclusions are considered to have trapped magma at the most differentiated stage.

7.4. A category of high-temperature alteration

The following alterations are recognized in C13 (Table 1): orthopyroxene in coarse hornblende is altered to clinopyroxene or cummingtonite (Fig. 4f) and actinolitic parts occur within coarse hornblende. In contrast to the alterations, fibrous actinolite occurs in coarse hornblende with titanite (Fig. 4g), flaky biotite occurs in coarse hornblende and biotite (Fig. 4h) and sealed microfractures are found in plagioclase (Fig. 4e) in C11 and C12 (Table 1).

The actinolitic alteration in C11 and C13 occurs at over 450°C, based on the equilibrium temperatures determined from the Holland and Blundy geothermometer (Fig. 7a). Fluid inclusions are sometimes found in the actinolitic parts around microfractures within the coarse hornblende of C11 and C12. Therefore, actinolitic alteration in coarse hornblende is considered to result from the fluid–mineral interaction. The temperature at which flaky biotite occurred was not examined because its determination would depend on oxygen fugacity (e.g. Wones and Eugster, 1965). In comparison, biotite in C11 and C12 shows more systematic relations between its mg-value and Si content than biotite in C13 (Fig. 5E). The sealed microfractures in plagioclase of C11 and C12 are composed of oligoclase, whose composition is close to those at the rims of the host plagioclase. Taking into account that there is no rim in plagioclase of C13, the sealed microfractures in plagioclase of C11 and C12 are considered to be formed below 500°C. The alterations observed in the three samples can be defined as a category of high-temperature alteration, which is contrary to the alteration observed in granitic rocks from other deep cores, which can be defined as a category of low-temperature alteration. In granitic rocks from other deep cores, a small amount of chlorite occurs on the surface of primary biotite (Kato and Sato, 1995). Chlorite, sericite, actinolite, anhydrite and epidote occur at the fractured parts of the rocks from other deep cores (Kato and Sato, 1995). The low-temperature alteration could proceed mainly at temperatures less than 350°C due to infiltration of the meteoric water (Kato and Sato, 1995). Thus, the alteration process is changing with decreasing temperature in the Kakkonda Granite.

8. Comparison of the determined temperatures at the sampling depths

The following three kinds of temperature determinations were compared at the sampling depths (Fig. 7b): the logged temperatures of Ikeuchi et al. (1998) (Fig. 3); homogenization temperatures of fluid inclusions reported by Komatsu et al. (1998); and equilibrium temperatures determined from the Fuhrman and Lindsley two-feldspar geothermometer in this study (Table 2).

Komatsu et al. (1998) carried out microthermometry of fluid inclusions in quartz of cutting samples collected from almost every 50 m depth interval of well WD-1a and rock of C13. The homogenization temperatures of fluid inclusions measured at 2900 and 2950 m depths were referred for C11 and those at 3200 and 3250 m depths were for C12. At depths of C11 and C12, liquid-rich inclusions are considered to trap the meteoric water (Komatsu et al., 1998), and therefore, the homogenization temperature could indicate the in situ temperatures without a fluid pressure correction (Fig. 7b). The depth of C13 is in a magmatic region without infiltration of the

meteoric water, where polyphase inclusions are exclusively found. In C13, some fluid inclusions have homogenization temperatures lower than the logged temperature of 500°C (Fig. 7b). Therefore, the fluid inclusions are considered to require a fluid pressure correction (possibly up to a lithostatic fluid pressure of 93 MPa using the assumption of a rock density of 2.5 g/cm^3). In the fluid pressure correction, inclusion fluids were approximated to fluids of the NaCl–H_2O system of Sourirajan and Kennedy (1962) and Bischoff and Pitzer (1989), and isocores of inclusion fluids were calculated using FLINCOR, a software of Brown (1989). The homogenization temperatures of 480–530°C were corrected to the trapping temperatures of 520–560°C through the fluid pressure correction (Fig. 7b,c).

Three equilibrium temperatures for Ab, Or and An components between pairs of K-feldspar and plagioclase (T_{Ab}, T_{Or} and T_{An}, respectively) were determined from the two-feldspar geothermometer (Table 2). In C11, the equilibrium temperatures of T_{Or} and T_{Ab} are slightly lower than the logged temperature and minimum homogenization temperature of liquid-rich inclusions (Fig. 7b). If the logged temperature and minimum homogenization temperature of liquid-rich inclusions indicate the in situ temperature at the sampling depth of C11, the two-feldspar geothermometer seems to indicate slightly lower equilibrium temperatures.

In C12, the T_{Ab} is slightly lower than the logged temperature, and the T_{Or} is slightly higher than the logged temperature (Fig. 7b). The T_{Ab} coincides with the minimum homogenization temperature of liquid-rich inclusions (Fig. 7b). The discordance between the T_{Ab} and T_{Or} could be attributed to the composition change of K-feldspar and/or albite lamella after perthite formation. Two possible processes to change the compositions of the minerals were considered as follows. If the minimum homogenization temperature of liquid-rich inclusions indicates the in situ temperature for C12, the T_{Ab} could be equal to the in situ temperature and T_{Or} could be higher than the in situ temperature. Based on the sensitivity of the calculation, the higher T_{Or} is attributed to a higher Or content in the albite lamella. The albite lamella might delay in exsolution of its Or component at the depth. On the contrary, if the logged temperature is correct for C12, albite lamella and K-feldspar are considered to increase in Or content and decrease in Ab content, respectively. This could result in higher T_{Or} and lower T_{Ab}, respectively. In this case, both minerals seem to be added potassium probably from K-rich fluids ascended from deeper levels.

In C13, the T_{Or}, T_{Ab} and T_{An} are slightly higher than the logged temperature and almost concordant with the homogenization temperatures of fluid inclusions with a fluid pressure correction (Fig. 7b). The equilibrium temperatures determined from the two-feldspar geothermometer possibly indicate the in situ temperature at the depth for C13.

Thus, the two-feldspar geothermometer indicates slightly lower equilibrium temperatures for C11, possibly concordant equilibrium temperatures for C12 and reasonable equilibrium temperatures for C13. The liquid-rich inclusions could indicate in situ temperatures at the depths of C11 and C12, and the polyphase inclusions probably require a fluid pressure correction to indicate the in situ temperature at the depth of C13. In C13, the Andersen and Lindsley magnetite–ilmenite geothermometer also indicates the in situ temperature in comparison to the corrected homogenization temperatures of fluid inclusions and equilibrium temperature determined from the two-feldspar geothermometer (Fig. 7c).

9. Conclusions

The Kakkonda Granite displays remarkable petrographic features initially formed just after solidification of magma as follows. Interstitial spaces of granite are not completely sealed. K-feldspar exhibits no perthite. Quartz includes glassy melt inclusions without devitrification. Hornblende is less intensively altered to actinolite, and biotite is not altered. The magnetite–ilmenite geothermometer of Anderson and Lindsley (1988) indicates equilibrium temperatures concordant with the in situ temperature of the sample over 500°C, and the two-feldspar geothermometer of

Fuhrman and Lindsley (1988) possibly indicates equilibrium temperatures over 410°C. In Kakkonda, the granitic magma began to be crystallized over 840°C and became solidified at 690–750°C. Later, magnetite exsolved ilmenite lamella at over 520°C, hornblende becomes actinolitic at over 450°C and K-feldspar formed perthite at 410–500°C. This study will lead to a better understanding of the cooling histories of outcropped granites.

Acknowledgements

This study was conducted as part of the 'Deep-Seated Geothermal Resources Survey' project at the Geological Survey of Japan (GSJ) and collaborated with the New Energy and Industrial Technology Development Organization (NEDO) and Japan Metals and Chemicals Co. Ltd. (JMC). We are very grateful to the NEDO for providing samples and to the staff of the JMC Geothermal Engineering Co. Ltd. (Geo-E) for useful discussions on the Kakkonda geothermal system. We also thank Drs. H. Shinohara and T. Takagi of the GSJ for their improvement of our earlier draft. Reviews and comments by Dr. P. Wood of the Institute of Geological and Nuclear Science, New Zealand and an anonymous reviewer resulted in a significant improvement in the presentation.

References

Anderson, D.J., Lindsley, D.H., 1988. Internally consistent solution models for Fe-Mg-Mn-Ti oxides: Fe-Ti oxides. Am. Mineral. 73, 714–726.

Bence, A.E., Albee, A.L., 1968. Empirical correction factors for electron microanalysis of silicate and oxides. J. Geol. 76, 382.

Bischoff, J.L., Pitzer, K.S., 1989. Liquid-vapor relations for the system NaCl-H_2O: summary of the P-T-x surface from 300° to 500°C. Am. J. Sci. 289, 217–248.

Brown, P.E., 1989. FLINCOR; a microcomputer program for reduction and investigation of fluid inclusion data. Am. Mineral. 74, 1390–1393.

Chappell, B.W., White, A.J.R., 1974. Two contrasting granite types. Pac. Geol. 8, 173–174.

Doi, N., Kato, O., Ikeuchi, K., Komatsu, R., Miyazaki, S., Akaku, K., Uchida, T., 1998. Genesis of the plutonic-hydrothermal system around Quaternary granite in the Kakkonda geothermal system, Japan. Geothermics 27, 663–690.

Frezzotti, M.L., 1992. Magmatic immiscibility and fluid phase evolution in the Mount Genis granite (Southeastern Sardinia, Italy). Geochim. Cosmochim. Acta 56, 21–33.

Fuhrman, M.L., Lindsley, D.H., 1988. Ternary-feldspar modeling and thermometry. Am. Mineral. 73, 201–215.

Fujimoto, K., Takahashi, M., Doi, N., Kato, O., 2000. High permeabilities of Quaternary granites in the Kakkonda geothermal area, northeast Japan. Proc. World Geothermal Congress 2000, pp. 1139–1144.

Giletti, B.J., Shanahan, T.M., 1997. Alkali diffusion in plagioclase feldspar. Chem. Geol. 139, 3–20.

Hanano, M., 1998. A simple model of a two-layered high-temperature liquid-dominated geothermal reservoir as a part of a large-scale hydrothermal convection system. Transp. Porous Media 33, 3–27.

Holland, T., Blundy, J., 1994. Non-ideal interactions in calcic amphiboles and their bearing on amphibole-plagioclase thermometry. Contrib. Mineral. Petrol. 116, 433–447.

Ikeuchi, K., Doi, N., Sakagawa, Y., Kamenosono, H., Uchida, T., 1998. High-temperature measurements in well WD-1a and the thermal structure of the Kakkonda geothermal system, Japan. Geothermics 27, 591–607.

Ishihara, S., 1977. The magnetite-series and ilmenite-series granitic rocks. Min. Geol. 27, 293–305.

Kanisawa, S., Doi, N., Kato, O., Ishikawa, K., 1994. Quaternary Kakkonda Granite underlying the Kakkonda geothermal field, northeast Japan (in Japanese with English abstract). J. Min. Petr. Econ. Geol. 89, 390–407.

Kasai, K., Sakagawa, Y., Komatsu, R., Sasaki, M., Akaku, K., Uchida, T., 1998. The origin of hypersaline liquid in the Quaternary Kakkonda Granite, sampled from well WD-1a, Kakkonda geothermal system, Japan. Geothermics 27, 631–645.

Kasai, K., Hishi, Y., Fukuda, D., Kato, O., Doi, N., Akaku, K., Ominato, T., Tosha, T., 2000. The fluid geochemistry and reservoir model for the Kakkonda geothermal system, obtained by NEDO's deep-seated geothermal reservoir survey, Japan. Proc. World Geothermal Congress 2000, pp. 1325–1330.

Kato, O., Doi, N., 1993. Neo-granitic pluton and later hydrothermal alteration at the Kakkonda geothermal field, Japan. Proc. 15th New Zealand Workshop, pp. 155–161.

Kato, O., Sato, K., 1995. Development of deep-seated geothermal reservoir bringing the Quaternary granite into focus in the Kakkonda geothermal field, northeast Japan (in Japanese with English abstract). Resour. Geol. 45, 131–144.

Kato, O., Okabe, T., Shigehara, S., Doi, N., Tosha, T., Koide, K., 2000. Permeable fractures and in-situ stress at the Kakkonda geothermal field, Japan. Proc. World Geothermal Congress 2000, pp. 1337–1342.

Komatsu, R., Ikeuchi, K., Doi, N., Sasaki, M., Uchida, T., Sasada, M., 1998. Characteristics of the Quaternary Kakkonda Granite and geothermal system clarified by fluid inclusion study of deep investigation well, Kakkonda, Japan

(in Japanese with English abstract). J. Geotherm. Res. Soc. Jpn. 20, 209–224.

Lagache, M., Weisbrod, A., 1977. The system: two alkali feldspar-KCl-NaCl-H_2O at moderate to high temperatures and low pressures. Contrib. Mineral. Petrol. 62, 77–101.

Leake, B.E., Woolley, A.R., Arps, C.E.S., Birch, W.D., Gilbert, M.C., Grice, J.D., Hawthorne, F.C., Kato, A., Kisch, H.J., Krivovichev, V.G., Linthout, K., Laird, J., Mandarino, J.A., Maresch, W.V., Nickel, E.H., Rock, N.M.S., Schumacher, J.C., Smith, D.C., Stephenson, N.C.N., Ungaretti, L., Whittaker, E.J.W., Youzhi, G., 1997. Nomenclature of amphiboles: report of the subcommittee on amphiboles of the international mineralogical association, commission on new minerals and mineral names. Can. Mineral. 35, 219–246.

Muraoka, H., Uchida, T., Sasada, M., Yagi, M., Akaku, K., Sasaki, M., Yasukawa, K., Miyazaki, S., Doi, N., Saito, S., Sato, K., Tanaka, S., 1998. Deep geothermal resources survey program: igneous, metamorphic and hydrothermal processes in a well encountering 500°C at 3,729 m depth, Kakkonda, Japan. Geothermics 27, 507–534.

Roedder, E., 1992. Fluid inclusion evidence for immiscibility in magmatic differentiation. Geochim. Cosmochim. Acta 56, 5–20.

Sasada, M., Miyazaki, S., Saito, S., 1993. NEDO's Deep-Seated Geothermal Resources Survey at the Kakkonda system, northeast Japan. Geotherm. Resour. Council Trans. 17, 181–185.

Sawaki, T., Sasaki, M., Fujimoto, K., Takeno, N., Tsukamoto, H., Sanada, K., Maeda, S., 2001. Corundum and zincian spinel from the Kakkonda geothermal system, Iwate Prefecture, northeastern Japan. J. Mineral. Petrol. Sci. 96, 137–147.

Smith, J.V., 1974. Diffusion. In: Feldspar Minerals, 2, Chemical and Textural Properties, Chapter 16. Springer, Berlin, 690 pp.

Sourirajan, S., Kennedy, G.C., 1962. The system H_2O-NaCl at elevated temperatures and pressures. Am. J. Sci. 260, 115–141.

Takeno, N., Muraoka, H., Sawaki, T., Sasaki, M., 2001. Thermodynamic framework of the contact metamorphism around the Kakkonda granite in an active geothermal field, northeast Japan. In: R. Cidu (Ed.), Proc. 10th Int. Symp. Water-Rock Interaction, vol. 1, pp. 765–768.

Tuttle, O.F., 1952. Origin of the contrasting mineralogy of extrusive and plutonic salic rocks. J. Geol. 60, 107–124.

Tuttle, O.F., Bowen, N.L., 1958. Origin of granite in the light of experimental studies in the system $NaAlSi_3O_8$-$KAlSi_3O_8$-SiO_2-H_2O. Geol. Soc. Am. Memoir 74, 1–153.

Uchida, T., Akaku, K., Sasaki, M., Kamenosono, H., Doi, N., Miyazaki, S., 1996. Recent progress of NEDO's 'Deep-Seated Geothermal Resources Survey' Project. Geotherm. Resour. Council Trans. 20, 643–648.

Wones, D.R., Eugster, H.P., 1965. Stability of biotite: experiment, theory, and application. Am. Mineral. 50, 1228–1272.

Wood, B.J., Banno, S., 1973. Garnet-orthopyroxene and orthopyroxene-clinopyroxene relationships in simple and complex systems. Contrib. Mineral. Petrol. 42, 109–124.

Yanagiya, S., Kasai, K., Brown, K.L., Giggenbach, W.F., 1996. Chemical characteristics of deep geothermal fluid in the Kakkonda geothermal system, Iwate prefecture, Japan (in Japanese with English abstract). Chinetsu 33, 1–18.